Metal oxide catalysts for the synthesis of covalent organic frameworks and one-step preparation of covalent organic framework-based composites

Yifan Zhu,[†1] Dongyang Zhu, [‡1] Qianqian Yan, [†] Guanhui Gao, [†] Jianan Xu, [†] Yifeng Liu, [†] Sampath B. Alahakoon, [†] Muhammad M. Rahman, [†] Pulickel M. Ajayan, [†] Eilaf Egap,* [†] and Rafael Verduzco*[†‡]

‡Department of Chemical and Biomolecular Engineering, Rice University, 6100 Main Street, MS-362, Houston, Texas 77005, United States

†Department of Materials Science and Nanoengineering, Rice University, 6100 Main Street, MS-325, Houston, Texas 77005, United States.

1 These authors contribute equally to the work.

ABSTRACT: The integration of covalent organic frameworks (COFs) with inorganic materials provides opportunities to develop a new class of composite materials with high surface areas and novel functionalities relevant to photocatalysis, chemical adsorption, and magnetic resonance imaging. However, current methods for the preparation of COF-based composites require challenging, multi-step synthetic protocols. Herein, we report a one-pot synthesis approach using a wide range of metal oxides to catalyze the synthesis of highly crystalline and porous covalent organic frameworks (COFs). We found that a large variety of metal oxides served as effective catalysts for the synthesis of imine COFs, including niobium (V) oxide (Nb_2O_5), nickel (II) oxide (NiO), manganese (IV) dioxide (MnO_2), ruthenium (IV) oxide (RuO_2), zinc (II) oxide (ZnO), lead (II) oxide (PbO), tellurium (IV) dioxide (TeO_2), tin (IV) oxide (SnO_2), manganese (III) oxide (Mn_2O_3), zirconium (IV) dioxide (ZrO_2) and aluminum (III) oxide (Al_2O_3). Nb_2O_5 was effective for the synthesis of a wide range of COFs with different functional groups and pore sizes, and these reactions produced a metal oxide/COF composite. By using Fe_3O_4 nanoparticles as the catalyst, we produced COF-based nanocomposites with Fe_3O_4 nanoparticles distributed throughout the final COF product. The Fe_3O_4/COF nanocomposite had a high surface area of 2196 m^2g^{-1}. This work demonstrates a class of novel, low-cost catalysts for synthesizing COFs and a new approach to produce metal oxide/COF composite materials.

Introduction

Covalent organic frameworks (COFs) are an emerging class of porous organic materials that have been widely developed for catalysis, optoelectronics, energy storage, pollutant removal, and drug delivery.[1–5] Integrating COFs with other functional materials, such as metal oxides,[6] perovskites,[7] and metal particles[8] results in composites that combine the high porosities and surface areas characteristics of COFs with the special physical and chemical properties of the functional materials.[9] In particular, the combination of metal oxides and COFs is useful for various applications including chemical adsorption and magnetic resonance imaging.[9] Furthermore, metal oxide/COF heterojunctions with excellent performance in photovoltaics and as photocatalysts could be designed through bandgap engineering of the composites.[6] However, current methods for the preparation of metal oxide/COF composites require elaborate, multi-step synthetic protocols. For example, one approach involves first synthetizing COFs and then growing metal oxides on the COF,[10,11] and alternative approaches involve forming or growing COFs on the surface of metal oxide particles[12] or substrates[13]. Simple physical mixing can result in aggregation or phase separation, resulting in poor performance or challenges in practical implementation.[9] Hence, there is a need for simple, effective, one-pot strategies for creating high-quality metal oxide/COF composites.

There is also a critical need for robust and low-cost catalysts for synthesizing high-quality COFs under mild reaction conditions.[14,15] For example, imine COFs are typically synthesized via reversible Schiff-base reactions under solvothermal conditions with acetic acid as the catalyst.[1] However, producing high-quality crystalline COFs requires tedious optimization of the reaction conditions for each set of monomers selected and commonly requires reaction time of several days and elevated temperatures.[16] Recent work has demonstrated that metal salts are effective catalysts for COF synthesis. Dichtel and coworkers reported that metal triflates, particularly $Sc(OTf)_3$, are robust catalysts for rapid synthesis of imine-based COFs at room temperature.[17] Verduzco and coworkers developed an ambient temperature synthesis approach for 2D and 3D COFs

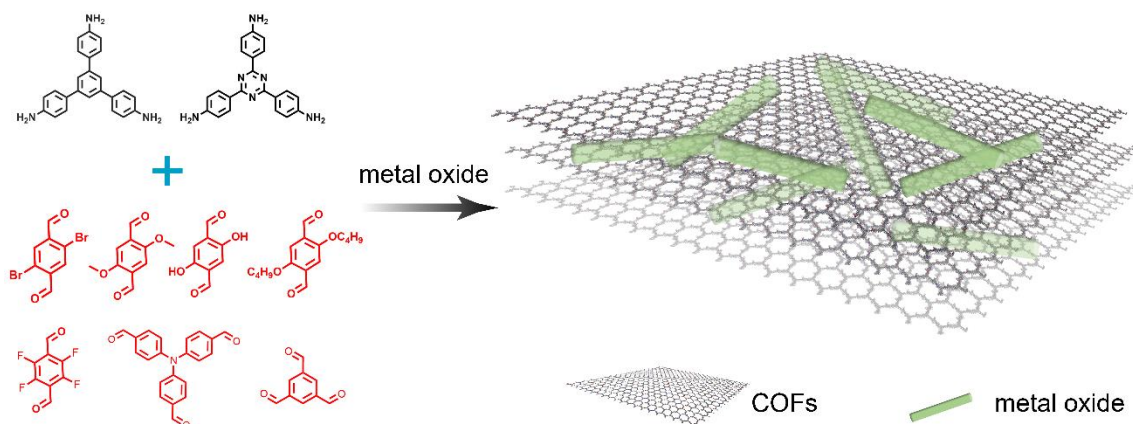using metal nitrate catalysts, and the approach was compatible with a large scope of functional groups.[18]

Figure 1. Schematic showing the synthesis of COFs using metal oxides.

Egap and coworkers presented a facile synthesis of COFs using lead halides and two-step methods to grow perovskite nanocrystals in the COF matrix.[7] While these approaches significantly broaden the catalyst library for COF synthesis, they cannot easily be applied to the preparation of COF-based composites.

Metal oxides consist of ordered surface arrays of Lewis acidic and basic sites that can provide multiple reactive binding sites or serve as catalytic sites.[19] The Lewis acidity of metal oxides enables them to be widely used as catalysts in various organic reactions,[20] such as nucleophilic substitution reactions of carboxylic acids,[21] selective oxidation of amine[22] and hydration reactions.[23] We hypothesized that metal oxides could catalyze the synthesis of imine COFs to produce COFs with excellent crystallinity and enable the preparation of metal oxide/COF composites in a one-pot reaction (Figure 1). Herein, we demonstrate the synthesis of metal oxide/COF composites by leveraging the strong Lewis acidity of a wide range of functional metal oxides, including Nb_2O_5, RuO_2, TiO_2, Mn_2O_3, and Fe_3O_4. All metal oxides tested produced composites of metal oxides and crystalline COFs, proving that this is a general approach for the synthesis of inorganic-organic composites. The COFs were synthesized with high yields with catalyst loadings ranging from 0.94 mol% - 188.1 mol%, enabling the preparation of metal oxide/COF composites with the ratio of COF to metal oxides dictated by the catalyst loading. We tested this synthetic approach for the synthesis of a series of imine COFs with different functionalities, and found excellent crystallinity for all COFs targeted. Furthermore, by using iron oxide (II, III) (Fe_3O_4) nanoparticles (NPs) as the catalyst, we were able to produce high-quality composites of Fe_3O_4 NPs and crystalline COFs. High-resolution transmission electron microscopy (HRTEM) analysis clearly revealed that the NPs were well-dispersed and embedded in the COFs interlayer space without compromising the morphology and size of NPs or the crystallinity of the COF. This "one-stone-two-birds approach" will significantly lower the barriers for the synthesis of COFs and enable the creation of COF-based nanocomposites.

Results and Discussions

To test the catalytic performance of metal oxides for synthesizing imine COFs, we initially focused on niobium(V) oxide (Nb_2O_5) as a catalyst for the synthesis of 1,3,5-tris(4-aminophenyl)benzene (TAPB) - 2,5-dimethoxyterephthaldehyde (OMePDA) (TAPB-OMePDA) COF. The polycondensation was conducted at 120 °C for three days using 1,2-dichlorobenzene and 1-butanol (volume ratio = 1:1) as the
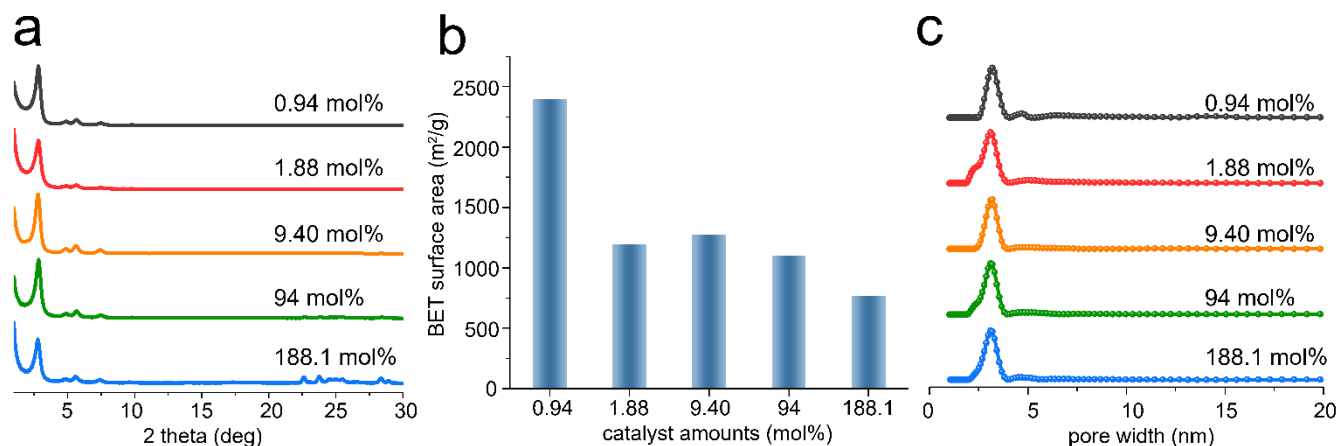

Figure 2. (a) PXRD spectra, (b) BET surface areas, and (c) Pore size distributions of TAPB-OMePDA COF samples synthesized using different catalyst loading of Nb_2O_5.
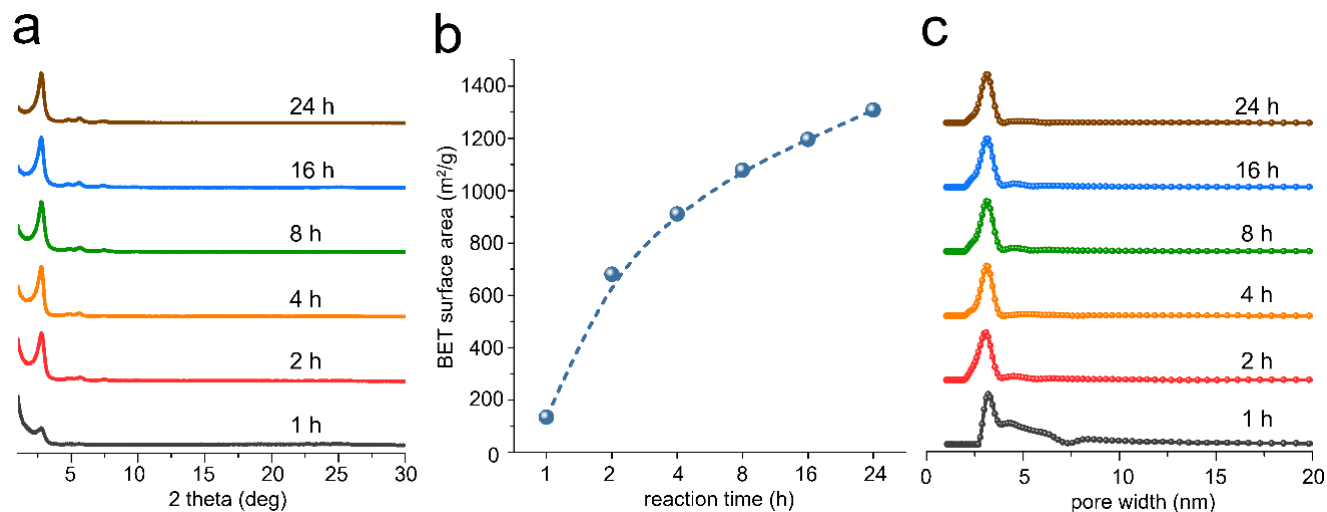
Figure 3. (a) PXRD spectra (b) BET surface areas, and (c) Pore size distributions of TAPB-OMePDA COF samples synthesized using 4.7 mol % Nb_2O_5 at different reaction time.

solvent system, and we varied the catalyst loading from 0.94 mol% to 188.1 mol% relative to amine monomers. Encouragingly, solid precipitates were observed upon the addition of Nb_2O_5, and the final material had excellent crystallinity, as reflected by sharp and prominent PXRD patterns of TAPB-OMePDA COFs obtained under different catalyst loadings (**Figure 2a**). The peaks ranging from 22º to 60º match with those of commercial Nb_2O_5 (**Figure S1**), while peaks at smaller angles reflect crystalline TAPB-OMePDA COF. Fourier-transform infrared spectroscopy (FT-IR) revealed the formation of an imine bond with the appearance of a C=N stretching located at 1618 cm⁻¹ along with the attenuation of the C=O and N–H stretch from the monomers (**Figure S2**). The Brunauer–Emmett–Teller (BET) surface areas of TAPB-DMTA COFs were determined through nitrogen sorption isotherms (**Figure S3**) and were 2405, 1202, 1280, 1105, 774 m² g⁻¹ (**Figure 2b**), for 0.94 mol%, 1.88 mol%, 9.4 mol%, 94 mol%, 188.1 mol% catalyst loadings, respectively. The measured surface areas decreased with increasing catalyst loadings, and this may reflect, in part, blockage of the micropores[7] by the Nb_2O_5 catalyst. All samples possessed narrow pore size distributions (**Figure 2c**), suggesting the formation of neat mesoporous structures and that no pore collapse occurred[24] even when doping with a large amount of metal oxides (> 94 mol%). With a low catalyst loading of 0.94 mol%, the surface area of COF products reached values as high as 2405 m² g⁻¹ even without supercritical CO_2 activation, which is among the highest reported values for a 2D COF,[7,14,17] suggesting an excellent catalytic efficiency for Nb_2O_5. At the same time, crystalline COFs could also be synthesized using much higher catalyst loadings of Nb_2O_5 (94.0 mol% and 188.1 mol%). This synthesis approach, therefore, is effective for producing Nb_2O_5/COF composites over a wide range of molar ratios of COF to Nb_2O_5 and with excellent crystallinity of the final COF product.

We performed further analysis of the composites prepared by 188.1 mol% N_2O_5 using scanning electron microscopy (SEM) and thermogravimetric analysis (TGA) to analyze the morphology and weight ratio of COF to metal oxide in the final material. SEM of this composite showcased a morphology of aggregated, disordered macroparticles, corresponding to the TAPB-OMePDA COF, while only a trace amount of metal oxides was observed on the surface (**Figure S4b and c**). We speculated that most metal oxides were encapsulated into the COF matrix during the formation of the frameworks. We performed TGA measurements in air to estimate the weight ratio of Nb_2O_5 to COFs in the composites. As shown in **Figure S5**, the organic components decomposed at around 370 °C, and the remaining mass corresponded to the amount of Nb_2O_5. The mass content of Nb_2O_5 was determined to be 28.5% in the composites. The initial mass percentage of Nb_2O_5 (43.7%) suggests that some metal oxides were removed during purification. Furthermore, by accounting for the mass of metal oxides in the final composite, the surface area of COFs in the composites was calculated to be 1082 m²g⁻¹.

Inspired by the successful catalytic performance of Nb_2O_5 in synthesizing highly crystalline COFs, we studied the kinetics of the formation of TAPB-OMePDA COFs. The precipitates were isolated at various reaction time intervals ranging from 1 h to 24 h, washed using centrifugation, and characterized by PXRD and BET (**Figure 3** and **Figure S6**). The crystallinity of the COF increased with reaction time. The COF prepared in 1 hour exhibited a shoulder peak located at 2.8º that corresponds to (100) peak in the PXRDs patterns (**Figure 3a**) and had a low BET surface area of 134 m² g⁻¹ (**Figure 3b**). The pore size distribution was relatively broad (**Figure 3c**), suggesting that poorly ordered structures with amorphous domains formed.[25,26] When the reaction time was increased from 2 h to 24 h, the (100) peak became sharper, and higher order (200) reflections gradually emerged in PXRD (**Figure 3a**). The BET surface areas also increased with reaction time from 680 m² g⁻¹ to 1308

m² g⁻¹ (**Figure 3b**), with narrowed and refined pore size distribution after 2 hours (**Figure 3c**). The enhanced porosity of COFs over time suggests the reorganization of ordered sheets[25] or amorphous polymer to form stacked structures[26] under the catalysis of Nb_2O_5.

To explore the universality of metal oxide catalysts for imine COF synthesis, we evaluated the catalytic performance of a series of metal oxides in the synthesis of TAPB-OMePDA COF. All the metal oxides we tested, including nickel (II) oxide (NiO), manganese (IV) dioxide (MnO_2), ruthenium (IV) oxide (RuO_2), zinc (II) oxide (ZnO), lead (II) oxide (PbO), tellurium (IV) dioxide (TeO_2), tin(IV) oxide (SnO_2), manganese(III) oxide (Mn_2O_3), zirconium (IV) dioxide (ZrO_2) and aluminum oxide (Al_2O_3), produced highly crystalline COFs with high yields of the final composite ranging from 65% to 95% (**Figure 4a-b, Table S1** and **Equation S1**). All the as-synthesized COFs exhibited high surface areas ranging from 697 m²g⁻¹ to 1644 m² g⁻¹, except for the ZrO_2 catalyzed sample which had a surface area of just 448 m² g⁻¹ (**Figure 4c-d**, **Figure S8-9**), and all the samples had a well-defined pore size distribution (**Figure S10**). We propose that the surface area and the yield of the final COF products might be determined by (1) the intrinsic Lewis acidity of metal cation, (2) the crystal structure of the metal oxides, and (3) the water tolerance of the metal oxides. In principle, metal cations with stronger Lewis acidity should more efficiently facilitate imine bond formation and imine exchange,[7] which are beneficial for producing high-quality, crystalline COFs. The crystal structures or phases of the metal oxides are related to the active Lewis acid surface sites and therefore the effective acidic catalytic activity.[20,27] This can also influence the stability of the catalysts.[20] Water generated during the formation of imine bonds can suppress Lewis acidity of metal oxides by hindering coordination,[21] and therefore metal oxides with good water tolerance such as Nb_2O_5 can lead to better catalytic performance.[20] We propose a catalytic mechanism involving coordination of the electron-rich oxygen in the aldehyde with the Nb^{5+}, which facilitates the attack of the carbonyl functional group by amine functionality. This mechanism for imine bond formation is shown in **Figure S12**, and SEM micrographs of the starting metal oxides prior to COF synthesis are provided in the Supporting Information (**Figures S20 – 29**).
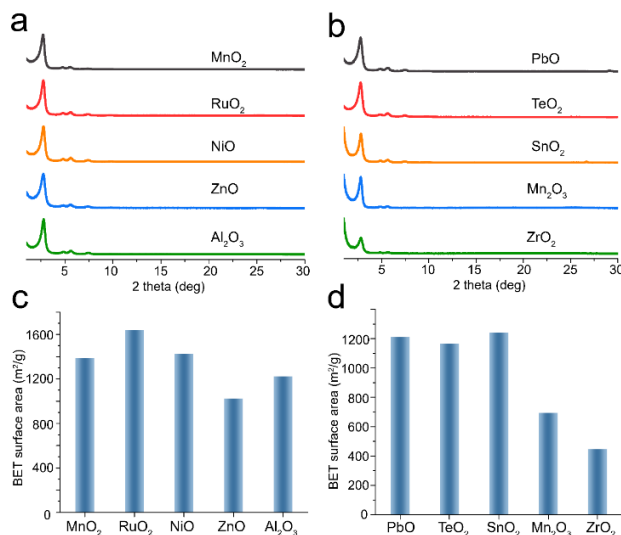
Figure 4. (a, b) PXRD spectra, (c, d) BET surface areas of TAPB-OMePDA COF samples synthesized using different metal oxides (catalysis loading = 4.7 mol%)

To understand the generality of metal oxide catalysts for the synthesis of imine COF-based composites, we further expanded the scope of monomers to generate COFs with different functional groups and topologies. Encouragingly, Nb_2O_5 catalyst showed excellent tolerance to a wide range of substituted aldehydes (-F, -Br, -OCH₃, -OH, -C₄H₉) and to amines with a triazine backbone. TAPB-BrPDA, TAPT-OMePDA, TAPT-OHPDA, TAPT-OTePDA, TAPT-FPDA were successfully synthesized with yields of 86%, 82%, 80%, 79%, 73%, respectively (**Table S2**). FT-IR spectroscopy confirmed the imine bond formation in the resulting solids, and no residual or unreacted monomers were observed (**Figure S13**). PXRD patterns of the above products exhibited prominent and narrow peaks that were consistent with previous studies,[7,14,17,18,24] suggesting excellent crystallinity of COFs synthesized using Nb_2O_5 catalysts (**Figure 5a-g**). The BET surface areas of TAPB-BrPDA, TAPT-OMePDA, TAPT-OHPDA, TAPT-OTePDA, TAPT-FPDA COFs were 1200 m²/g, 1027 m²/g, 1959 m²/g, 1411 m²/g, 1960 m²/g, respectively, which were comparable to those reported for similar COFs synthesized *via* acetic acid catalysis (**Figure 5h-i**). For example, the surface areas of TAPT-OHPDA and TAPT-OMePDA COF were 709 m²/g⁻¹ [28] and 1258 m²/g⁻¹ [24] when using acetic acid as the catalyst and a similar workup using vacuum drying of the final materials. A comparison of previously synthesized COFs along with the materials reported in this study are provided in the Supporting Information **Table S3**. In addition to the "3 + 2" node-linker topology, we also successfully synthesized TAPT-BTCA and TAPT-TFPA COFs with a "3 + 3" node-linker geometry using Nb_2O_5 catalyst. These COFs have a much smaller pore size, 1.13 nm for TAPT-BTCA COF compared to 3.3 nm for TAPB-OMePDA COF[24]. Highly crystalline TAPT-TFPA and TAPT-BTCA COFs were successfully produced with high surface areas of 1550 m²g⁻¹ and 939 m²g⁻¹, respectively, demonstrating the excellent versatility of metal oxides for catalytic use. We also note that all TAPT-based COFs had

excellent crystallinities when synthesized using Nb_2O_5 catalysts. This may be due to the coordination of nitrogen atoms of triazine groups with the catalyst surface and the electron lone pairs of TAPT occupying the orbital of cationic metal centers,[29] which can assist in the formation of docking sites and facilitate the attachment and growth of successive layers.[30]

Finally, we explored the preparation of well-defined COF-based nanocomposites in a one-pot reaction using Fe_3O_4 NPs (30 nm) as the catalyst. Upon the addition of Fe_3O_4 NPs (65 mol%) into the solution of TAPB and OMePDA monomers, precipitates were obtained immediately. The synthesized COF exhibited sharp PXRD peaks at

2.8° corresponding to that of TAPB-OMePDA COFs (**Figure S15**). Moreover, the nanocomposites possessed a high surface area of 2196 m² g⁻¹ (**Figure S16**). TGA showed the weight ratio of Fe_3O_4 NPs in the final composites was approximately 9.65% (**Figure S17**). Through X-ray photoelectron spectroscopy (XPS) survey scans, we observed peaks at 284, 397 and 532 eV, which corresponded to the C1s, N1s, and O1s binding energies, respectively. No apparent peaks related to Fe were observed, (**Figure S17**) and we did not observe any PXRD peaks related to Fe_3O_4 NPs since pure Fe_3O_4 NPs cannot be detected by PXRD (**Figure S15**). XPS elemental scan detected Fe in the composite (**Figure S18 and S19**), but the content of
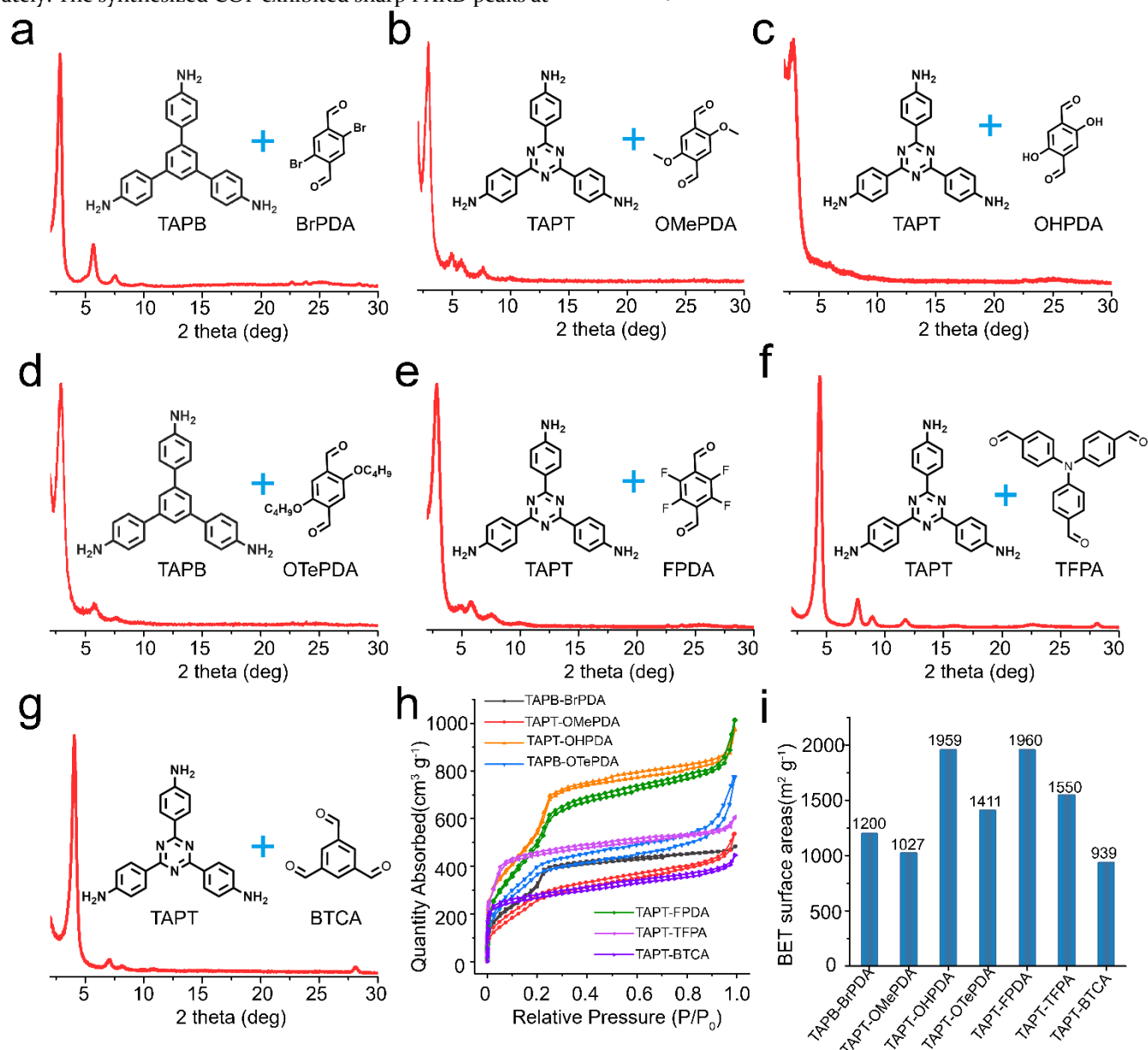

Figure 5. Synthesis of different COFs using 4.7 mol% Nb_2O_5 catalyst. (a-g) PXRD spectra for different COFs synthesized using Nb_2O_5; (h) Nitrogen sorption isotherms; and (i) BET surface areas for different COF samples. OMePDA = 2,5-dimethoxyterephthalaldehyde, TFPA = tris(4-formylphenyl)amine, TAPB = 1,3,5-tris(4-aminophenyl)benzene, TAPT = 2,4,6-tris(4-aminophenyl)-1,3,5-triazine, BrPDA = 2,5-dibromoterephthalaldehyde, FPDA = 2,3,5,6-tetrafluoroterephthalaldehyde, OHPDA = 2,5-dihydroxy-1,4-benzenedicarboxaldehyde, OTePDA = 2,5-dibutoxyterephthalaldehyde, and BTCA = benzene-1,3,5-tricarbaldehyde.

Fe was determined to be only 0.07 atom%. The relatively low loading of Fe_3O_4 NPs from XPS elemental scan suggested that NPs were encapsulated inside COF rather than on the surface of COFs, as XPS is a very surface-sensitive technique. This was further confirmed by transmission electron microscopy (TEM) analysis. TEM images (**Figure 6a**) show that a number of nanoparticles (Fe_3O_4 NPs) were embedded in the large 2D sheets (TAPB-OMePDA COFs). The Fe_3O_4 NPs were uniformly distributed and had well-defined spherical shapes in COF layered structures (**Figure**

6b,c). HRTEM further confirmed that Fe_3O_4 NPs were well-dispersed in the COF matrix, and the size of NPs remained unchanged (around 30 nm) after the reaction (**Figure 6d, e**). As the size of NPs was larger than the pore size of COFs, the Fe_3O_4 NPs likely resided in the COF interlayer space or the micropores.[7] The well dispersed NPs and uniform elemental distribution of Fe were further confirmed by high-angle annular dark-field scanning transmission electron microscopy (HAADF-STEM) and elemental mapping (**Figure 6f-k**).
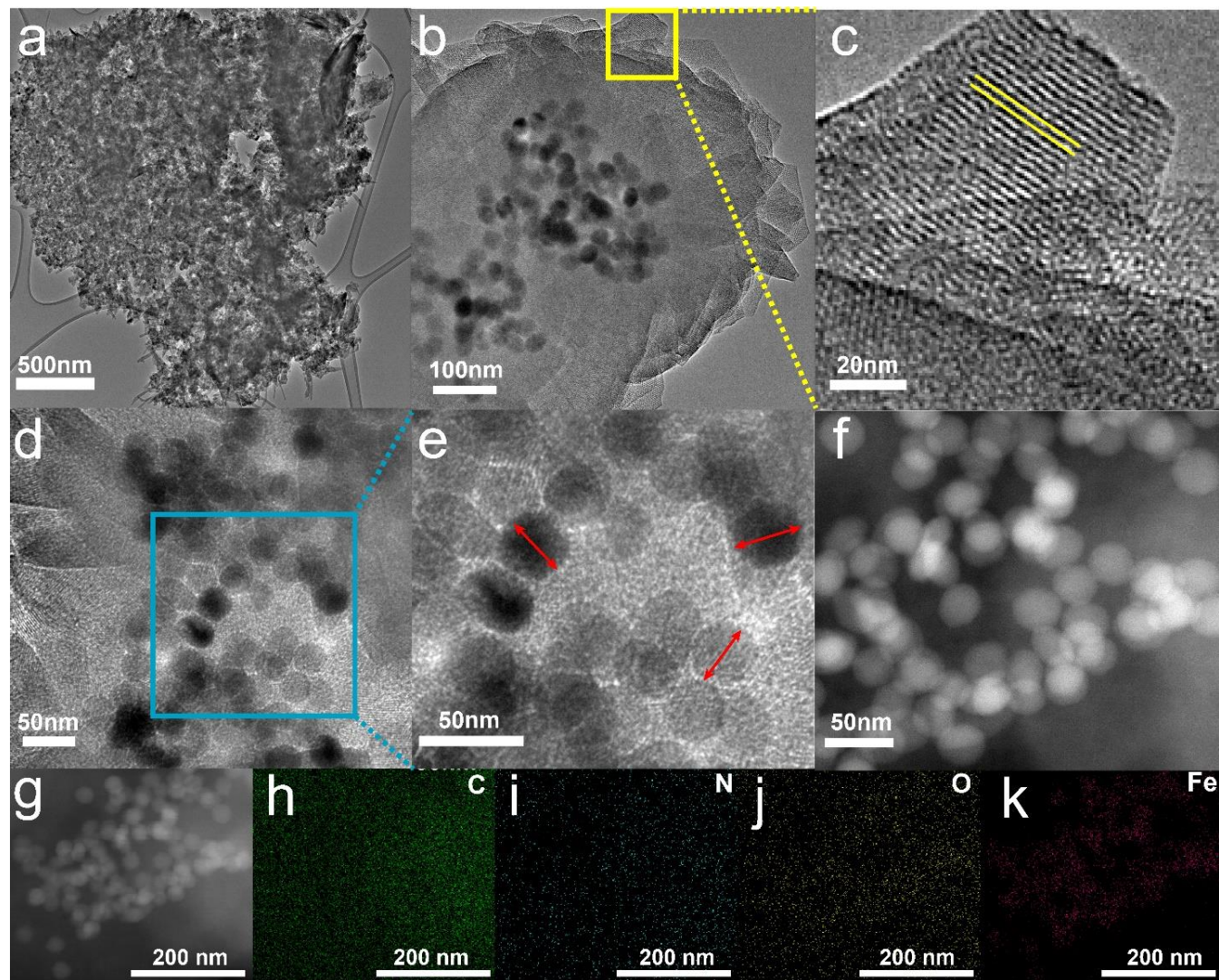

Figure 6. TEM analysis of Fe_3O_4/COF nanocomposites. (a) TEM images of nanocomposites formed by Fe_3O_4 nanoparticles and TAPB-OMePDA COFs. (b) HRTEM showing Fe_3O_4 NPs embedded between COF interlayers; (c) Enlarged selected areas from yellow box showing the lattice fringes of COFs; (d, e) well-defined Fe_3O_4 NPs with spherical shapes embedded between COF sheets; e is the enlarged selected area from the blue box in d; (f, g) HAADF-STEM; (h-k) Elemental mapping of selected areas in (g).

Conclusion

In conclusion, we demonstrated the excellent catalytic performance of metal oxides in the synthesis of highly crystalline imine COFs. A large variety of metal oxides were tested in the synthesis of TAPB-OMePDA imine COFs, and all were successful in producing crystalline COF products with high surface areas. We also demonstrated that Nb2O5 could successfully catalyze the synthesis of COFs with different functional groups and pore sizes. The metal oxides were encapsulated in situ during COF synthesis, resulting in the preparation of a metal oxide/COF composite. We demonstrated that Fe3O4 nanoparticles catalyzed imine

COF formation and produced well-defined Fe₃O₄/COF nanocomposites with high surface areas and without compromising the size or integrity of the nanoparticles. This work demonstrates new, low-cost catalysts for COF synthesis and provides a novel approach to create functional hybrid materials potentially with unique electronic, optical, and magnetic properties.

EXPERIMENTAL SECTION

General procedure for the synthesis of COF and metal oxide/COF composites. We provide a description of the synthesis of TAPB-OMePDA COFs, and the same general approach was used to synthesize the different COFs and COF-based composites described. TAPB (0.04 mol) and OMePDA (0.06 mmol) were weighed and dissolved in a mixture of 0.5 mL of 1-butanol and 0.5 mL of 1, 2-dichlorobenzene in a Pyrex tube. Before the tube was sealed, the corresponding amount of metal oxide was added, and the solution was sonicated for 10 min. The sealed tubes were then transferred into an oven and heated at 120 °C for 3 days. All of the products were separated and washed thoroughly using THF and acetone. For vacuum drying, final solids were washed and immersed in hexane prior to drying. After filtration, samples were dried in vacuum oven under 80 °C overnight. For the various COFs synthesized, the monomer ratio was chosen such that there was an equimolar ratio NH2 and CHO groups in the reaction mixture.

Instrumentation. PXRD patterns were collected from Rigaku SmartLab X-ray diffractometer with Cu Kα1 radiation. Samples were analyzed at a scan speed of 1.0 deg/min. FT-IR spectra were recorded on a Nicolet FT-IR Infrared Microscope. HRTEM was performed on a Titan Themis Scan/Transmission Electron Microscope operated at 300 kV. Samples were briefly sonicated prior to being dropped on the grids. Nitrogen sorption isotherms were measured on Quantachrome Autosorb-iQ3-MP/Kr BET Surface Analyzer. Samples were degassed under vacuum at 120 °C for 12 h prior to the nitrogen sorption measurements that were performed in a liquid nitrogen bath at 77 K. Multi-point BET plots were collected from 0.05-0.2 P/Po range and pore size distributions were determined using quenched solid density functional theory (QSDFT) model (N2 at 77 K on carbon, cylindrical pores) using the instrument software. XPS was performed on a PHI Quantera XPS, which used a focused monochromatic Al Kα X-ray (1486.7 eV) source for excitation. The 50 W, 15 kV and 200 μm diameter X-rays were shoot on the sample. The XPS survey scan spectra in the 1100 – 0 eV binding energy range were recorded in 0.5 eV steps with a pass energy of 140 eV. High resolution scan spectra were recorded in 0.1 eV steps with a pass energy of 26 eV. Low energy electrons and Ar⁺ ions were conducted for specimen neutralization in each measurement.

ASSOCIATED CONTENT

Supporting Information

Supporting Information: materials and methods, experimental details, additional characterization data including PXRD, FTIR, nitrogen sorption tests, TEM, TGA, XPS and SEM.

AUTHOR INFORMATION

Corresponding Author

*(E.E.) E-mail: eilaf.egap@rice.edu

*(R.V.) E-mail: rafaelv@rice.edu.

Author Contributions

1 These authors contribute equally to the work.

REFERENCES

(1) Huang, N.; Wang, P.; Jiang, D. Covalent Organic Frameworks: A Materials Platform for Structural and Functional Designs. *Nat. Rev. Mater.* **2016**, *1* (10), 16068.

(2) Côté, A. P.; Benin, A. I.; Ockwig, N. W.; O'Keeffe, M.; Matzger, A. J.; Yaghi, O. M. Chemistry: Porous, Crystalline, Covalent Organic Frameworks. *Science.* **2005**, *310* (5751), 1166–1170.

(3) Wang, H.; Wang, H.; Wang, Z.; Tang, L.; Zeng, G.; Xu, P.; Chen, M.; Xiong, T.; Zhou, C.; Li, X.; Huang, D.; Zhu, Y.; Wang, Z.; Tang, J. Covalent Organic Framework Photocatalysts: Structures and Applications. *Chem. Soc. Rev.* **2020**, *49* (12), 4135–4165.

(4) Zhu, D.; Xu, G.; Barnes, M.; Li, Y.; Tseng, C.; Zhang, Z.; Zhang, J.; Zhu, Y.; Khalil, S.; Rahman, M. M.; Verduzco, R.; Ajayan, P. M. Covalent Organic Frameworks for Batteries. *Adv. Funct. Mater.* **2021**, 2100505.

(5) Zhu, D.; Zhu, Y.; Yan, Q.; Barnes, M.; Liu, F.; Yu, P.; Tseng, C.-P.; Tjahjono, N.; Huang, P.-C.; Rahman, M. M.; Egap, E.; Ajayan, P. M.; Verduzco, R. Pure Crystalline Covalent Organic Framework Aerogels. *Chem. Mater.* **2021**, *33* (11), 4216–4224.

(6) Zhang, M.; Lu, M.; Lang, Z.; Liu, J.; Liu, M.; Chang, J.; Li, L.; Shang, L.; Wang, M.; Li, S.; Lan, Y. Semiconductor/Covalent-Organic-Framework Z-Scheme Heterojunctions for Artificial Photosynthesis. *Angew. Chemie Int. Ed.* **2020**, *59* (16), 6500–6506.

(7) Liu, Y.; Zhu, Y.; Alahakoon, S. B.; Egap, E. Synthesis of Imine-Based Covalent Organic Frameworks Catalyzed by Metal Halides and in Situ Growth of Perovskite@COF Composites. *ACS Mater. Lett.* **2020**,*2*(12), 1561–1566.

(8) White, R. J.; Luque, R.; Budarin, V. L.; Clark, J. H.; Macquarrie, D. J. Supported Metal Nanoparticles on Porous Materials. Methods and Applications. *Chem. Soc. Rev.* **2009**, *38* (2), 481–494.

(9) Liu, Y.; Zhou, W.; Teo, W. L.; Wang, K.; Zhang, L.; Zeng, Y.; Zhao, Y. Covalent-Organic-Framework-Based Composite Materials. *Chem* **2020**, *6* (12), 3172–3202.

(10) Zhang, Y.; Hu, Y.; Zhao, J.; Park, E.; Jin, Y.; Liu, Q.; Zhang, W. Covalent Organic Framework-Supported Fe-TiO2 Nanoparticles as Ambient-Light-Active Photocatalysts. *J. Mater. Chem. A* **2019**, *7* (27), 16364–16371.

(11) Wang, H.; Jiao, F.; Gao, F.; Huang, J.; Zhao, Y.; Shen, Y.; Zhang, Y.; Qian, X. Facile Synthesis of Magnetic Covalent Organic Frameworks for the Hydrophilic Enrichment of N - Glycopeptides. *J. Mater. Chem. B* **2017**, *5* (22), 4052–4059.

(12) Tan, J.; Namuangruk, S.; Kong, W.; Kungwan, N.; Guo, J.; Wang, C. Manipulation of Amorphous-to-Crystalline Transformation: Towards the Construction of Covalent Organic Framework Hybrid Microspheres with NIR Photothermal Conversion Ability. *Angew. Chemie - Int. Ed.* **2016**, *55* (45), 13979–13984.

(13) Lu, H.; Wang, C.; Chen, J.; Ge, R.; Leng, W.; Dong, B.; Huang, J.; Gao, Y. A Novel 3D Covalent Organic Framework Membrane Grown on a Porous α-Al2O3 Substrate under Solvothermal Conditions. *Chem. Commun.* **2015**, *51* (85), 15562–15565.

(14) Feriante, C. H.; Jhulki, S.; Evans, A. M.; Dasari, R. R.; Slicker, K.; Dichtel, W. R.; Marder, S. R. Rapid Synthesis of High Surface Area Imine-Linked 2D Covalent Organic Frameworks by Avoiding Pore Collapse During Isolation. *Adv. Mater.* **2020**, *32* (2), 1905776.

(15) Hu, J.; Zanca, F.; McManus, G. J.; Riha, I. A.; Nguyen, H. G. T.; Shirley, W.; Borcik, C. G.; Wylie, B. J.; Benamara, M.; van Zee, R. D.; Moghadam, P. Z.; Beyzavi, H. Catalyst-Enabled *In Situ* Linkage Reduction in Imine Covalent Organic Frameworks. *ACS Appl. Mater. Interfaces* **2021**, *13* (18), 21740–21747.

(16) Lohse, M. S.; Bein, T. Covalent Organic Frameworks: Structures, Synthesis, and Applications. *Adv. Funct. Mater.* **2018**, *28* (33), 1705553.

(17) Matsumoto, M.; Dasari, R. R.; Ji, W.; Feriante, C. H.; Parker, T. C.; Marder, S. R.; Dichtel, W. R. Rapid, Low Temperature Formation of Imine-Linked Covalent Organic Frameworks Catalyzed by Metal Triflates. *J. Am. Chem. Soc.* **2017**, *139* (14), 4999–5002.

(18) Zhu, D.; Zhang, Z.; Alemany, L. B.; Li, Y.; Nnorom, N.; Barnes, M.; Khalil, S.; Rahman, M. M.; Ajayan, P. M.; Verduzco, R. Rapid, Ambient Temperature Synthesis of Imine Covalent Organic Frameworks Catalyzed by Transition-Metal Nitrates. *Chem. Mater.* **2021**, *33* (9), 3394–3400.

(19) Metiu, H.; Chrétien, S.; Hu, Z.; Li, B.; Sun, X. Chemistry of Lewis Acid-Base Pairs on Oxide Surfaces. *J. Phys. Chem. C* **2012**, *116* (19), 10439–10450.

(20) Siddiki, S. M. A. H.; Rashed, M. N.; Ali, M. A.; Toyao, T.; Hirunsit, P.; Ehara, M.; Shimizu, K. Lewis Acid Catalysis of Nb₂O₅ for Reactions of Carboxylic Acid Derivatives in the Presence of Basic Inhibitors. *ChemCatChem* **2019**, *11* (1), 383–396.

(21) Ali, M. A.; Siddiki, S. M. A. H.; Kon, K.; Hasegawa, J.; Shimizu, K. Versatile and Sustainable Synthesis of Cyclic Imides from Dicarboxylic Acids and Amines by Nb2O5 as a Base-Tolerant Heterogeneous Lewis Acid Catalyst. *Chem. - A Eur. J.* **2014**, *20* (44), 14256–14260.

(22) Furukawa, S.; Ohno, Y.; Shishido, T.; Teramura, K.; Tanaka, T. Reaction Mechanism of Selective Photooxidation of Amines over Niobium Oxide: Visible-Light-Induced Electron Transfer between Adsorbed Amine and Nb2O5. *J. Phys. Chem. C* **2013**, *117* (1), 442–450.

(23) Van Dijk, A. J. M.; Duchateau, R.; Hensen, E. J. M.; Meuldijk, J.; Koning, C. E. Polyamide Synthesis from 6-Aminocapronitrile, Part 2: Heterogeneously Catalyzed Nitrile Hydrolysis with Consecutive Amine Amidation. *Chem. - A Eur. J.* **2007**, *13* (27), 7673–7681.

(24) Zhu, D.; Verduzco, R. Ultralow Surface Tension Solvents Enable Facile COF Activation with Reduced Pore Collapse. *ACS Appl. Mater. Interfaces* **2020**, *12* (29), 33121–33127.

(25) Feriante, C.; Evans, A. M.; Jhulki, S.; Castano, I.; Strauss, M. J.; Barlow, S.; Dichtel, W. R.; Marder, S. R. New Mechanistic Insights into the Formation of Imine-Linked Two-Dimensional Covalent Organic Frameworks. *J. Am. Chem. Soc.* **2020**, *142* (43), 18637–18644.

(26) Smith, B. J.; Overholts, A. C.; Hwang, N.; Dichtel, W. R. Insight into the Crystallization of Amorphous Imine-Linked Polymer Networks to 2D Covalent Organic Frameworks. *Chem. Commun.* **2016**, *52* (18), 3690–3693.

(27) Wachs, I. E.; Chen, Y.; Jehng, J. M.; Briand, L. E.; Tanaka, T. Molecular Structure and Reactivity of the Group V Metal Oxides. *Catal. Today* **2003**, *78*, 13–24.

(28) Qian, H. L.; Dai, C.; Yang, C. X.; Yan, X. P. High-Crystallinity Covalent Organic Framework with Dual Fluorescence Emissions and Its Ratiometric Sensing Application. *ACS Appl. Mater. Interfaces* **2017**, *9* (29), 24999–25005.

(29) Wang, Q.; Zheng, C.; Zhang, J.; He, F.; Yao, Y.; Zhang, T. C.; He, C. Insights into the Adsorption of Pb(II) over Trimercapto-s-Triazine Trisodium Salt-Modified Lignin in a Wide PH Range. *Chem. Eng. J. Adv.* **2020**, *1*, 100002.

(30) Xiong, C.; Ning, H.; Jia, G.; Hong, X.; Fei, X.; Donglin, J. Towards Covalent Organic Frameworks with Predesignable and Aligned Open Docking Sites. *Chem. Commun.* **2014**, *50* (46), 6161–6163.

Table of Contents (ToC) Graphic